Evaluation of the CMORPH High-Resolution Precipitation Product for Hydrological Applications over South Korea

Jungho Kim[1,2] and Heechan Han[3]

1 Cooperative Institute for Research in the Atmosphere (CIRA), Colorado State University, Fort Collins, Colorado, U.S.A.
2 NOAA Earth System Research Laboratory, Physical Sciences Laboratory, Boulder, Colorado, U.S.A.
3 Department of Civil and Environmental Engineering, Colorado State University, Fort Collins, Colorado, U.S.A.

Correspondence: Jungho Kim (Email: Jungho.Kim@noaa.gov)

Submitted to *Atmospheric Research*

Abstract

The use of a high-resolution satellite-based precipitation product on a global-scale is attractive to hydrological applications. However, it should be systematically evaluated from various perspectives as the quality property is dependent on the geographical and topographical features of a region. This study comprehensively assesses the Climate Prediction Center morphing technique (CMORPH) precipitation product over South Korea. Two evaluation approaches, the general evaluation using statistical metrics and the detection evaluation (to measure skill in detecting precipitation and non-precipitation) using categorical metrics, are employed based on an 18-year long-term period of record. As a result, the CMORPH product tended to underestimate precipitation over South Korea, and the level of the underestimation varied with the seasons and regions. The overall quality was adequate for hydrological applications that require precipitation data at the annual-to-daily resolution but not at hourly resolution. Skill in detecting hourly precipitation in a storm event was 60% of the rain-gauge data, and the accuracies of total volume and peak value were 45% and 40%, respectively. The quality in the coastal regions and islands was not as good as in inland areas at low altitudes. The accuracy in a wet season was better than that in a dry/winter season. Notably, the CMORPH precipitation product was not suitable for snowfall data. Ultimately, the CMORPH product at hourly resolution needs a correction process using the local measurement systems for enhancing the quality property over South Korea.

Keywords: High-resolution satellite precipitation product; CMORPH; Multi-temporal evaluation; Hydrological application; South Korea

1. Introduction

The role of precipitation is significant in hydrological processes (Sorooshian et al., 2011; Alijanian et al., 2017; Yao et al., 2020). Precipitation is measured from various observing systems on the ground and space. Thus, understanding the properties of measurement data is fundamental to know the uncertainty and reliability (AghaKouchak et al., 2011). Rain-gauge data is considered as the ground truth but does not accurately represent the spatial distribution of precipitation owing to the inherent weakness of point measurement, observation density, and restrictive environments to install an observing instrument (Kim and Yoo, 2014). On the other hand, a weather radar provides the spatial distribution of precipitation estimate, which is better than that from a rain-gauge system but is also subject to limitations in estimating the accurate precipitation due to beam blockage, beam filling, beam overshoot effects, mixed-phase precipitation, ground returns, rain-path attenuation, and variations in the rainfall drop size distribution (Stampoulis and Anagnostou, 2012; Kim et al., 2015a). From this point of view, the advent of satellite-based precipitation datasets is attractive to various applications as it has many benefits compared to the two observing systems. This study aims to assess a high-resolution satellite-based precipitation product from various perspectives comprehensively.

Up to date, a number of the satellite-based precipitation products have been developed, including the Tropical Rainfall Measuring Mission (TRMM, Huffman et al., 2007), the Precipitation Estimation from Remotely Sensed Information using Artificial Neural Networks method (PERSIANN, Hsu et al., 1997), and the National Oceanic and Atmospheric Administration (NOAA) Climate Prediction Center morphing technique (CMORPH, Joyce et al., 2004). Undoubtedly for the last two decades, they have advanced physical sciences and modeling in hydrology under the seamless gridded data feature and the long-term historical records on a large-

scale (Zeweldi et al., 2011; Sun et al., 2016). They have also been considered the only credible alternative to complementing precipitation measurements from the rain-gauge and weather radar observing systems (Li and Shao, 2010; Jones et al., 2015; Chao et al., 2018).

Among the satellite-based precipitation products, the CMORPH is considered a high-resolution precipitation data as it provides the global precipitation measurement at 8 km by 8 km and 30-minute resolution. As input data, the features meet the requirements of most hydrological applications. Many studies have employed the CMORPH for studying physical processes and modeling in the hydrologic cycle (Pan et al., 2010; Zeweldi et al., 2011), numerical weather prediction (Ebert et al., 2007), crop monitoring (Romaguera et al., 2010), and rainfall erosivity mapping (Kim et al., 2020). However, it is questionable whether the CMORPH provides fully qualified precipitation data worldwide (Peña Arancibia et al., 2013; Bayissa et al., 2017). In the same context, operational and decision-making applications tend not to integrate the satellite-based precipitation products into their system because of a lack of information regarding the associated uncertainties and reliability of these products (Bitew and Gebremichael, 2011; Liechti et al., 2012). In general, the performance of the satellite-based precipitation products varies significantly with different factors. The first factor is related to the inherent features of the products. The product's spatial and temporal resolutions are significant for their application's purpose and scope (Yao et al., 2020). It is a well-known fact that the performance is better at coarse resolution than at higher resolution (Peng et al., 2020). The retrieval algorithm and system as the inherent feature are also important to determine the accuracy of the satellite precipitation products as the CMORPH proved to perform better than the satellite reanalysis data, such as Climate Hazards Group Infrared Precipitation with Stations. The second factor is the features of the application regions (Yao et al., 2020). It is a challenge to keep the quality of satellite-based products consistent regardless of

regions because various geographical and topographical features of the globe affect the detecting ability of sensors on satellites (Yilmaz and Derin, 2014). From this point of view, the evaluation of satellite-based products should be documented to the extent possible to establish confidence for users by focusing on the application area before applying the products to their areas of concern (Tan et al., 2015).

In general, the properties of the CMORPH have been verified based on statistical metrics to quantify the accuracy and on categorical metrics to measure skill in detecting precipitation for various regions: South America (Salio et al., 2015), Malaysia (Tan et al., 2015), Ethiopia (Hirpa et al., 2009), Iran (Katiraie-Boroujerdy et al., 2013; Moazami et al., 2016; Alijanian et al., 2017), Tibetan plateau (Gao and Liu, 2013), and China (Jiang et al., 2010; Jiang et al., 2016; Sun et al., 2016). The previous studies' consistent findings are that the property depends on the regions in different geographical and topographical features and that the performance increases as temporal resolution decreases. This result well describes the need to evaluate the CMORPH precipitation product for understanding the uncertainty and reliability before employing it to a specific region such as the Korean Peninsula.

On the other hand, the studies evaluated the CMORPH precipitation product by comparing it with the rain-gauge data at different coarse resolutions from annual to daily. Therefore, the information about the strength and weakness of the CMORPH precipitation product from the hourly and event-based perspectives is limited. Besides, most studies measured precipitation accuracy with the lumped metrics, which cannot capture the variability by seasons that determine precipitation in some regions.

This study presents here a comprehensive assessment of the CMORPH precipitation product over South Korea. The efficient management of water resources and early warning

systems for extreme events is a challenge as most storms come from three sides of the sea over the peninsula. Also, owing to 70% of the total area characterized by the mountainous regions, the ground-based measurement systems cannot provide the consistent quality of precipitation data all over South Korea. Hence, the use of the high-resolution satellite-based precipitation products is attractive from these perspectives. The goal is to assess its capability as precipitation data for hydrological applications. Not only coarse resolution (annual-to-daily) but also hourly resolution is considered. The event-based evaluation is also conducted to examine the usefulness of the CMORPH precipitation product for precipitation cases rather than non-precipitation cases. The assessment of the qualitative and quantitative properties is implemented using statistical and categorical metrics. Wet and dry periods are considered to explore the strength and weakness of the CMORPH precipitation product in different seasonal variations. Rain-gauge data as a reference value is classified into four groups in different regions and elevations to assess the CMORPH precipitation product's quality properties in different geographical and topographical features.

The rest of this paper is organized as follows: Section 2 introduces application materials and methods. Section 3 represents the evaluation results based on various temporal resolutions from yearly to hourly and rain-gauge locations. Section 4 describes the overall assessment of the CMORPH precipitation product and the findings.

2. Material and Methods

2.1 Application Area and Data

South Korea located in the center of east Asia is selected as an application area, lying between latitudes 33°~39° N. and longitudes 124°~130° E. The total area is approximately 99,373 km^2. South Korea is the southern area of the Korean Peninsula surrounded by water on three sides, the

Yellow Sea to the west, the East Sea to the east, and the South Sea to the south, and thus vulnerable to storms coming from the three seas at all seasons (Kim et al., 2015b; Kim and Joo, 2015). Fig. 1 shows the application domain, digital elevation model (DEM), and 48 rain-gauge locations used in this study.

Figure 1

South Korea has four seasons with its climatic features, spring from March to May, Summer from June to August, Fall from September to November, and Winter from December to February (Kim et al., 2015b). The annual average temperature is 14.5° Celsius, the hottest month is August as the monthly average temperature of 25 ° Celsius, and the coldest month is January at -7° Celsius. The range of annual precipitation is roughly from 1,000 to 1,850 mm (1,270 mm on average). In general, a wet season is from June to September, and 70% of annual precipitation occurs during this season owing to the monsoon and typhoons (Kim and Joo, 2015). A period from October to February is referred to as a dry season, and from November to February is referred to as a snow-dominated season (Joo et al., 2015).

The terrain is mostly complex and mountainous so that it is not easy to install rain-gauge instruments on the ground and employ weather radars due to beam blockage (Kim et al., 2014; 2015a). South Korea has two mountain ranges, Taebaeksanmaek and Sobaeksanmaek, as shown in Fig. 1. The Taebaeksanmaek mountains are located along South Korea's eastern edge and run along the eastern coast. The Sobaeksanmaek mountains are a mountain range cutting across the southern region of South Korea. The two mountain ranges divide South Korea into three regions, the West, East, and South regions (hereinafter West, East, or South region), having different types

of dominated precipitation during a winter season. The West and East regions are snow-dominated during the winter due to the cold front and snowstorms from the north's Siberian continental air-mass. The South region is warm in all seasons compared to the other two regions and barely snows during the winter.

Total 48 rain-gauges precipitation data from the Korea Meteorological Administration (https://data.kma.go.kr/cmmn/main.do) are used as a reference data set to evaluate the CMORPH precipitation product on the same location. Long-term data from 1998 to 2015 year is used in this study. A rain-gauge data and the CMORPH gridded data covering the area of the rain-gauge location are paired. The original temporal resolution of the rain-gauge data used in this study is an hourly time step. This study implemented a simple aggregation process to upscale it to produce the daily-to-annual rain-gauge data for the CMORPH evaluation.

In addition, it should be addressed about a matter of some concern to a discrepancy between the spatial resolutions of a rain-gauge and the CMORPH precipitation, affecting the CMORPH assessment. The importance of understanding the discrepancy and its effects on evaluating the gridded precipitation products (e.g., weather radar and satellite) has been recognized for decades (Hendrick and Comer, 1970; Zawadzki, 1973; Harrold et al., 1974; Ciach and Krajewski, 1999). Many previous studies confirmed that the effect of the discrepancy on the gridded precipitation assessment depends on temporal resolutions (Ciach and Krajewski, 1999; Villarini et al., 2008; Yang et al., 2016). In general, the effect increased as the temporal resolution increased. High temporal resolutions under an hour time step were affected by the discrepancy of the spatial resolutions of the two datasets, but the effect in coarser temporal resolutions over an hour time step was not apparent (Ciach and Krajewski, 1999; Gabriele et al., 2008; Kim et al., 2014). Some studies attempted to reduce errors arising from the effect of the discrepancy by matching the spatial

resolution of a rain-gauge with a gridded precipitation data. Habib et al. (2012) and Li et al. (2019) employed the spatial interpolation methods to upscale rain-gauge precipitation data, corresponding to the satellite precipitation data's spatial resolution. However, the spatial interpolation methods to upscale rain-gauge data should be carefully implemented because its performance depends on a rain-gauge network density. It could generate other errors in ungauged areas (Kim et al., 2020). Since this study aims to evaluate the CMORPH precipitation product in hour-to-annual temporal resolutions, this study assumes that the effect is not significant in the CMORPH evaluation process.

A range of altitudes of the rain-gauges is from 11 to 773 m, indicating that the rain-gauges are spatially distributed in low and high areas. Also, a fraction of the rain-gauges is located in coastal regions near the three seas and Jeju-island. The total rain-gauges are divided into four groups depending on geographical and topographical features: Group1 is located near a coastal region including Jeju island, Group2 located on under 100 m, Group3 located on between 100~200 m, and Group4 located on over 200 m.

2.2 CMORPH precipitation product

The CMORPH is a high-resolution global precipitation product, with a history longer than ground-based remote sensing data such as weather radars. The CMORPH produces global precipitation estimates at an 8 km × 8 km resolution every 30 min. Overall, this technique exclusively uses precipitation estimates derived from low Earth orbit (LEO) satellite-derived passive microwave (PWM) observations (Joyce et al., 2004; Xie et al., 2017; Kim et al., 2020). As the coverage of the PMW-based retrievals is severely limited in the half-hour window owing to the spatial and temporal sampling natures of LEO satellites (even when multiple satellites are used), the CMORPH takes advantage of the high temporal resolution of the geostationary satellite infrared

(IR) imagery to create motion vectors for the cloud systems. It subsequently applies the cloud motion vectors to the available PMW-based retrievals to produce continuous precipitation estimates over the entire globe. At each half-hour window, the IR data availability is almost guaranteed at a given location and can be used to extract the spatial propagation of precipitation features. For additional details regarding the CMORPH technique, interested readers are referred to Xie et al. (2017) and Chen et al. (2020).

The entire CMORPH dataset in version 1.0 is reprocessed and extended to cover 1998 to the present. The reprocessing includes a bias correction using gauge data (Xie et al., 2017). The reprocessing includes a bias correction using gauge data. According to Xie et al. (2017), the bias correction process is implemented for the raw CMORPH through probability density function (PDF) matching against the CPC daily gauge analysis over land and through adjustment against the Global Precipitation Climatology Project (GPCP) pentad merged analysis of precipitation over ocean. The bias-corrected CMORPH exhibits improved accuracy in representing the spatial distribution patterns and temporal variations of precipitation over the global domain. Among three types of precipitation estimates from the CMORPH, 30-min/8 km, 3-hr/0.25°, and 1-day/0.25°, this study used the CMORPH in the highest temporal and spatial resolution, and each 30-min estimate is accumulated to obtain the hourly precipitation. Four temporal resolutions, annual, monthly, daily, and hourly, are used, and the hourly precipitation evaluation includes the event-based evaluation results.

2.3 Evaluation Strategy

2.3.1 Metrics

This study employs the two evaluation approaches, quantitative evaluation using statistical metrics and detection evaluation (to measure skill in detecting precipitation) using categorical metrics. For the quantitative evaluation, seven metrics are used (see Table 1): correlation coefficient (CC), Nash-Sutcliffe efficiency (NSE), percent-bias (PBIAS), root mean square error (RMSE), volume error (VE), peak error (PE) and time error (TE). CC exhibits a trend of estimated precipitation against observations, NSE shows the magnitude of the estimated error variance compared to the observed data variance (Han et al., 2019; Kim et al., 2019), PBIAS shows a ratio of the sum of residuals to the sum of observed data and RMSE indicates the standard deviation of the residuals between estimated and observed data. CC, NSE, PBIAS, and RMSE measure the general accuracy of the CMORPH precipitation data, and VE, PE, and TE are used as additional metrics for the event-based evaluation.

Table 1

For the detection evaluation, three categorical metrics are employed: Probability of detection (POD), False Alarm Ratio (FAR), and Critical Success Index (CSI) (Ebert et al., 2007; Jiang et al., 2016). These categorical metrics measure skill in detecting precipitation and no-precipitation in the unit time (e.g., hourly). POD (eq. 1) describes the fraction of the number of precipitations correctly identified by the CMORPH data to the total number of precipitation occurrences observed by rain-gauge data. The POD ranges from 0 to 1; 0 indicates no skill, and 1 indicates a perfect score. The FAR (eq. 2) corresponds to the fraction of cases identified by the CMORPH data but not confirmed by rain-gauge data. The CSI (eq. 3) combines different aspects of the POD and FAR, describing the overall fraction of the precipitation occurrences correctly

identified by the CMORPH data in all cases. The CSI ranges from 0 to 1; 0 indicates no skill, and 1 indicates perfect skill.

The three categorical metrics can be represented by equations as follows:

$$\mathrm{POD} = \frac{t_H}{t_H + t_M} \quad (1)$$

$$\mathrm{FAR} = \frac{t_F}{t_H + t_F} \quad (2)$$

$$\mathrm{CSI} = \frac{t_H}{t_H + t_M + t_F} \quad (3)$$

Here, t_H, t_M, and t_F are total cases corresponding to each case.

Table 2

Table 2 shows the most common 2x2 form of the contingency table to evaluate all possible precipitation cases. In the table, Hit (H) and Miss (M) indicate a case of the CMORPH correctly and incorrectly detecting precipitation while precipitation is observed from the rain-gauge, respectively. False Alarms (F) indicates a case of the CMORPH detecting precipitation while precipitation is not observed from the rain-gauge.

2.3.2 Classification of A Storm Event

For the event-based evaluation, a process to classify a storm event is required to separate and identify independent storm events from an entire period of data. This study employs a classification

framework developed by the United States Department of Agriculture to define and classify an independent storm event (Kim et al., 2020). Fig. 2 shows the conceptual diagram of the classification method initially developed for estimating rainfall erosivity.

Figure 2

Conditions to classify an independent storm event are as follows:

- Total precipitation (P) is more than 12.7 mm: P >= 12.7 mm
- When a storm has precipitation more than 6.35 mm in 30 min, it can be classified as an independent storm event even though total precipitation is less than 12.7 mm
- Inter-event time definition (IETD) is 6 hours, indicating that between two individual storm events over 12.7 mm needs no precipitation duration for 6 hours at least.
- When total precipitation for 6 hours or greater than that is less than 12.7 mm, precipitation can be ignored.

3. Results

3.1. Coarse Resolution Evaluation

3.1.1. Annual Precipitation

Fig. 3 shows the evaluation results of the annual precipitation, consisting of (a) a comparison of the annual areal average precipitations between the CMORPH and rain-gauge data, (b) the 10-90th percentile range of relative error (%) for all rain-gauge locations, (c) a scatter plot of the annual precipitations in the dry and wet years and (d) the probability density functions (PDFs) of the four statistical metrics.

Figure 3

In Fig. 3a, the CMORPH mean areal precipitation was well-matched with the rain-gauge data, especially in terms of representing a change (e.g., increasing and decreasing trends) of the annual precipitation by year, but consistently underestimated in all years. Numerically, a level of underestimation was around 10 % on average. In Fig. 3b, the 10-90th percentiles range of relative errors was formed around ±30%, indicating that the quantitative accuracy greatly varied with the verification locations. This result suggests that various geographical and morphological features might affect the detecting ability of sensors on satellites.

In Fig. 3c, a dry year is defined as a year in which the annual precipitation is less than 30-year mean annual precipitation (1981-2010), and a wet year is just the opposite year. Regardless of dry or wet years, the CMORPH tended to underestimate the annual precipitation against the rain-gauge data, especially in a wet year. From the regression lines, the annual precipitations in wet and dry years are biased around 16% and 5%, respectively. Notably, fractions of CC>0.70 and

NSE>0.0 were higher than 85% (see Fig. 3d). The median value of PBIAS was -8.6%, indicating the CMORPH annual precipitation is underestimated. The median value of RMSE was 227.8 mm/yr, corresponding to 17.9% of the 30-years mean annual precipitation.

Figure 4

In Fig. 4, the spatial distributions of CCs and PBIADs were relatively uniform, but NSE and RMSE were not uniform. Overall, the quality of the CMORPH annual precipitation in inland regions was better than that in coastal regions, and it was apparent from the NSE and RMSE results. Notably, in coastal regions, the CMORPH annual precipitation had lower values in correlation (CC<0.70) and negative NSE values. RMSEs were higher than 500.0 mm/yr, corresponding to 39% of the 30-years mean annual precipitation. The PBIAS result confirmed that the annual precipitation in inland regions tended to have a low bias within ±10%, but that in coastal regions showed overestimation, especially in Jeju island.

3.1.2. Monthly Precipitation

The evaluation results of the CMORPH monthly precipitation data are shown in Fig. 5. Fig. 5 a-c are the same as Fig. 4 a-c. Fig. 5d, a radial graph, demonstrates the monthly medium values and 10-90th percentile ranges of the four statistical metrics. In Fig. 5a, the trend of monthly precipitation by seasonality was quite similar to the rain-gauge data, and the monthly difference was only 7.9 mm/month on average. In Fig. 5b, the variability of the relative errors in a dry season was broader than that in a wet season as the range was around ±100% in a dry season but ±50% in a wet season. As expected, it is confirmed that the CMORPH monthly precipitation in a dry season is more biased than that in a wet season (see Fig. 5c). In Fig. 5d, the overall property of CMORPH monthly precipitation was quite different in the seasons. Remarkably, the dry months tended to have lower CCs, negative NSEs, and PBIASs with high variability than those in the wet months. However, higher RMSEs were observed in the significant wet months, from July to September, owing to a relatively higher monthly precipitation.

Figure 5

Fig. 6 shows the spatial distributions of the statistical metrics of the CMORPH monthly precipitation. It consists of (a) January for a dry month, (b) August for a wet month, and (c) 12-month total period results to explore the quality depending on the seasons. In (a) January result, the spatial distributions were not uniform, and the spatial features could be divided into three by the regions, i.e., the West, East, and South, defined by the mountain ranges, Taebaeksanmaek and Sobaeksanmaek. The South region had higher CCs and NSEs and lower PBIASs compared to the West and East regions. This result is associated with a dominant type of precipitation as

precipitation is different depending on the regions during the winter. There are three primary reasons for that.

Figure 6

The first one is the Siberian air-mass coming from the north and making a cold front on the northern area of the Sobaeksanmaek mountain ranges, while the South region is usually affected by a warm front from the south sea. Hence, the South region is much warmer than the West and East regions during the winter season. The second one is the two mountain ranges that block a cold front and snow clouds coming into the South region. The third one is that the South region is affected by a low-pressure system formed in the warm South Sea so that rain is the dominant precipitation regardless of seasons. Therefore, the West and East regions are snow-dominated areas during the winter season. The South region is a rain-dominated area regardless of seasons and barely have snow during the winter season. These results suggest that the CMORPH snow data quality might not be as good as that of the CMORPH rain data.

Notably, the CMORPH monthly precipitation in January was considerably underestimated in Jeju island, where rain is the dominant precipitation in all seasons. The correlation is high, the same as that in the South region, but the PBIAS result suggests that the amount of the CMORPH monthly precipitation is around 50% of the rain-gauge data. Because the four rain-gauge locations are affected by water as the locations are near the sea and the CMORPH grid covers both the land and seawater. This is a well-known fact that the CMORH precipitation tends to have lower accuracy in the area near the water. For instance, Kim et al. (2020) found that the CMORPH tended to overestimate precipitation near waterbodies in the United States. However, the result of this

study showed the opposite case to underestimate precipitation. This finding is important as it confirms the quality of the satellite precipitation product depending on the region. Overall, RMSEs were under 30 mm/month, and higher values were observed in the East and South coastal regions and Jeju island.

Fig. 6b shows the results in August as a representative of wet months. The spatial distributions of the four statistical metrics are uniform, compared to the results in January. All CCs and NSEs are above 0.7 except that in Jeju island. Most PBIASs were close to zero, indicating a low bias. As expected, the CMORPH tended to underestimate precipitation in Jeju island and the South Sea's coastal regions. The RMSEs higher than 120 mm/month were observed in most coastal regions and inland regions at high altitudes.

Fig. 6c shows the averaged results for all months. Overall, features of the spatial distributions were similar to the results in August. It is an understandable result as most results (9 months) except that in the winter months (3 months) showed better quality. The averaged RMSE is 59 mm/month over South Korea, and RMSEs in coastal regions and Jeju island were higher than that in inland regions.

3.1.3. Daily Precipitation

Fig. 7 shows the daily precipitation evaluation results, consisting of (a) a comparison of fractions of no-precipitation and precipitation detected from the rain-gauge and CMORPH data, (b) a comparison of fractions of daily precipitation at every 5 mm/day interval (50 mm/day in the figure indicates an interval of values greater than 50 mm/day), and (c) a distribution chart of fractions of relative error (%).

Figure 7

A fraction of days with precipitation is around 25%, and that with non-precipitation is around 75% in both precipitation datasets, and it decreased as precipitation increased (see Fig. 7a, b). Notably, there was only a little difference between the CMORPH and rain-gauge data, indicating skill in detecting precipitation is remarkable from the perspective of probability. In Fig. 7c, the 25-75th percentiles range of relative error was from -53% to 150%, and the median value was 4.2%. The relative errors were densely formed in a range of negative values and be sparely formed in a range of positive values. This result suggests that the CMORPH daily precipitation has a high possibility of being underestimated with low variability and a low possibility of being overestimated with high variability.

Figure 8

Fig. 8 shows the spatial distributions of the four statistical metrics of daily precipitation in dry and wet seasons. Same as the monthly results, the quality property of the CMORPH daily

precipitation in a wet season was better than that in a dry season, and the spatial distribution patterns varied with the seasons. In a wet season, most rain-gauge locations represented CC>0.7, NSE>0.4, and -10<PBIAS<10, except for some of the coastal regions and Jeju island locations. The overall quality was the lowest in the East region regardless of the seasons. For the same reasons described in the monthly precipitation evaluation section, the South region has a better PBIAS pattern than other regions in a dry/winter season.

3.2. High-Resolution Evaluation

3.2.1. Hourly Precipitation

This section addresses the evaluation results of the CMORPH hourly precipitation in the four groups. Fig. 9 shows the Box and Whisker plot, representing the four quartiles ranges and medium value of the statistical metrics in two seasons. As expected, the quality was better in a wet season as the median CCs were formed around 0.5, but 0.3 in a dry season. The 25-75th percentiles range of NSEs in a wet season was narrowly formed around 0.0, indicating that the quality of the CMORPH hourly precipitation is regarded as comparable as that of the averaged rain-gauge precipitation is. However, most NSEs in a dry season were formed in a broader range of negative values. Considering the results at all temporal resolutions, the performance decreased as the resolution increased, which is a general result. Regardless of the groups, the quality properties in a wet season were better than that in a dry season.

Figure 9

From PBIAS results, it is firmly confirmed that the CMORPH product tended to underestimate hourly precipitation regardless of the seasons and groups. In all cases, the 25-75th percentiles of PBIAS are ranged from -20 to -3.5%. RMSEs in a wet season are higher than those in a dry season, which is considered an understandable result as higher rainfall is commonly observed in a wet season. The median RMSE was 1.2 mm/hr in a wet season. Depending on the four groups, the statistical metrics' properties were not entirely different in a wet season, but in a dry season a range. Group 1 and 2 showed lower and wider metrics than those in the other two groups in lower elevation regions, especially those observed in CC, PBIAS, and RMSE results. Among the rain-gauge locations showing the lower quality, most rain-gauges were located in coastal regions and Jeju island. Group 4 at high altitudes showed slightly low NSEs and a more comprehensive PBIAS range, but it was not significant.

Figure 10

Fig. 10 shows POD, FAR, and CSI results for the four groups and seasons to examine skill in detecting precipitation and non-precipitation regardless of intensity. In all seasons, most PODs were ranged from 0.30 to 0.70. The median value was 0.44, meaning that correctly detected precipitation accuracy is 44% on average. The accuracy in a wet season (51% on average) was higher than that in a dry season (32%). In a dry season, there were no objectionable differences of PODs depending on the groups. However, in a wet season, there was a noticeable difference between Group 1 and 4 (coastal and inland regions at high altitudes) and Group 2 and 4 (inland regions at low altitudes). The difference was 10% on average. These results suggest that skill in detecting precipitation varies with geographical and topographical features of a region.

FARs were higher in a dry season, indicating that the rate of failure to detect hourly precipitation and non-precipitation is high. Nevertheless, there were no objectionable differences between the four groups. The mean value of the median FARs in the four groups was 0.64. In other words, among 100 hours of precipitation cases identified by the CMORPH, 64 hours were not with precipitation, which is incorrect detection cases. Regardless of the four groups and seasons, CSIs were ranged from 0.2 to 0.5, and the median value was 0.33. In other words, among 100 hours of complex cases (including non-precipitation and precipitation) identified by the CMORPH, 33 hours were correctly observed as non-precipitation and precipitation. Like the other metrics, CSIs in a wet season were higher than those in a dry season, and the difference was 0.2 (20%) on average.

The results above addressed skills in detecting precipitation and in identifying non-precipitation without considering precipitation intensity. Fig. 11 shows POD, FAR, and CSI results in different intensities. Skill in detecting various precipitation intensities is verified. Thresholds ranging from 0.5 to 5.0 mm/hr are applied by increasing 0.1 mm/hr. The results represent a change of the median values by thresholds. According to the three categorical metrics results, the skill was the highest at 0.5 mm/hr and then decreased as the threshold increased. A notable difference among the groups was not observed, but the skill in Group 1 was slightly lower than the other groups, especially in a wet season. The difference in the skills in two seasons seems like a systematic form consistent in all thresholds.

Figure 11

3.2.2. Event-Based Precipitation

The event-based evaluation focuses on verifying skills in detecting an individual storm event and in measuring precipitation features. A fraction of the detected storm events, total volume, peak value, and timing errors are considered the precipitation features. Fig. 12 shows the evaluation results of skill detection in detecting individual storm events. In Fig. 12a, the fraction is a ratio of storm events detected by the CMORPH to the rain-gauge data. The detected storm event is defined as a case where the CMORPH detects at least an hour of precipitation for a storm event. For example, the CMORPH in Group 1 detected 76.7% of storm events while was not able to detect even an hour of precipitation for 23.3% of storm events. A fraction of detected storm events was 78.3% on average and not considerably varied with the groups. Fig. 12b shows the PDFs of the storm events by duration, and the CMORPH and rain-gauge results are compared for the four groups and total. Overall, the PDFs were well matched, and the difference between the two datasets in the four groups was relatively small.

Figure 12

Figure 13

Fig. 13 shows the evaluation results of timing error for the detected storm events. The timing error is defined as a ratio of incorrectly detected times of a storm event to the actual duration identified by the rain-gauge data. For instance, the CMORPH detects 7 hours of precipitation to a storm event with a duration of 10 hours, indicating the timing error is 30%. The identified storm events are classified into three types of a storm event by the duration (d), $0<d<12$, $12<d<24$, $24<d<36$, and $d>36$. Fig. 13a shows a representative PDF result of the timing errors for $12<d<24$

in Group 1. Overall, the PDF was similar to a normal distribution form, and it suggests that the mean value and standard deviation of the PDF were meaningful to analyze the features of the timing error. The mean and standard deviation values of the PDFs by the duration and group are analyzed in Fig. 13 c-d below.

Fig. 13b shows a fraction of 0% (when the CMORPH correctly detected a storm event's precipitation for all duration) timing error cases by the duration. As expected, a fraction decreased as the duration increased. The fractions were under 5% for a storm event with over 12 hours of duration. Group 1 represented the lowest fraction at all durations, but the other three groups were quite similar. In Fig. 13c and d, the mean and standard deviation values decreased as duration increased, indicating that a storm event with a shorter duration has lower errors and variations. Group 1 had the highest mean value and variance than the other three groups, and Group 2 and 3 were considered the better groups.

Figure 14

Fig. 14 shows the evaluation results of total volume and peak value errors and RMSE from the four groups' detected storm events. It consists of two parts, (a) PDFs of the errors and (b) features (e.g., the 1st and 3rd quantiles and median values) of the PDFs. In the total volume error result, the CMORPH tended to underestimate a storm event's total precipitation as Q1 and Q3 were in a range of negative values. The median value was around -45%, indicating that the CMORPH measured only 45% of the storm event's total precipitation compared to the rain-gauge data. The median peak error was around -40.0%, suggesting that the CMORPH precipitation data might not be suitable for analyzing extreme cases. The median RMSE was -4.3 mm, meaning the CMORPH

hourly precipitation error during a storm event. All errors in Group 1 were slightly higher than the others.

4. Discussion and Conclusions

This study implemented the CMORPH precipitation product's assessment at the annual-to-hourly resolutions from various perspectives of the hydrological applications over South Korea. The preliminary results are as follows:

1) The quality properties of the CMORPH precipitation data varied with temporal resolutions. The CMORPH annual-to-daily precipitation data met the requirements for hydrological applications, while the hourly precipitation was not as good as the coarse precipitation data. Notably, the CMORPH tended to underestimate precipitation regardless of temporal resolutions. These results suggest that the CMORPH precipitation data is useful for water resources management and long-term hydrologic simulations that require the coarse resolution of precipitation. However, it is not appropriate for hydrologic applications that require the hourly resolution of precipitation at least.
2) The accuracy of the CMORPH precipitation data to detect and estimate precipitation in a storm event was not satisfied. The median total error of a storm event was around 45% of the rain-gauge data, and the peak error was 40%. A level of skill in detecting precipitation and non-precipitation was 60% of the rain-gauge data.
3) The quality of the CMORPH precipitation was affected by geographical features and seasons. Regardless of temporal resolutions, the CMORPH precipitation in the coastal

regions and islands was not as good as in inland areas, especially at low altitudes. Also, the CMORPH precipitation data in a wet season was better than that in a dry season.

Ultimately, the CMORPH hourly precipitation data need to correct a bias for enhancing the quality over South Korea. The bias correction should be implemented based on assessing the CMORPH precipitation data as conducted in this study. We expect that the assessment in this study will help understand the property of the CMORPH precipitation data over South Korea and support further studies.

Acknowledgments

This work was supported by the NOAA Physical Sciences Laboratory and Colorado State University. And this research was supported by Basic Science Research Program through the National Research Foundation of Korea

References

AghaKouchak, A., Behrangi, A., Sorooshian, S., Hsu, K., Amitai, E., 2011. Evaluation of satellite-retrieved extreme precipitation rates across the central United States. J. Geophys. Res. 116, D02115.

Alijanian, M., Rakhshandehroo, G.R., Mishra, A.K., Dehghani, M., 2017. Evaluation of satellite rainfall climatology using CMORPH, PERSIANN-CDR, PERSIANN, TRMM, MSWEP over Iran. International Journal of Climatology 37, 4896-4914.

Bayissa, Y., Tadesse, T., Demisse, G., Shiferaw, A., 2017. Evaluation of satellite-based rainfall estimates and application to monitor meteorological drought for the upper Blue Nile basin,

Ethiopia. Remote Sensing 9, 669.

Bitew, M.M., Gebremichael, M., 2011. Evaluation of satellite rainfall products through hydrologic simulation in a fully distributed hydrologic model. Water Resources Research 47. W06526.

Chao, L., Zhang, K., Li, Z., Zhu, Y., Wang, J., Yu, Z., 2018. Geographically weighted regression based methods for merging satellite and gauge precipitation. J. Hydrol. 558, 275-289.

Chen, H., Chandrasekar, V., Cifelli, R., Xie, P., 2019. A machine learning system for precipitation estimation using satellite and ground radar network observations. IEEE Trans. Geosci. Remote Sens. 58, 982-994.

Ebert, E.E., Janowiak, J.E., Kidd, C., 2007. Comparison of near-real-time precipitation estimates from satellite observations and numerical models. Bulletin of the American Meteorological Society 88, 47-64.

Gao, Y.C., Liu, M.F., 2013. Evaluation of high-resolution satellite precipitation products using rain gauge observations over the Tibetan Plateau. Hydrology & Earth System Sciences 17, 837-849.

Han, H., Kim, J., Chandrasekar, V., Choi, J., Lim, S., 2019. Modeling streamflow enhanced by precipitation from Atmospheric River using the NOAA National Water Model: A case study of the Russian river basin for February 2004. Atmosphere 10, 466.

Hirpa, F.A., Gebremichael, M., Hopson, T., 2009. Evaluation of high resolution satellite precipitation products over very complex terrain in Ethiopia. J. Appl. Meteorol. Clim. 49, 1044-1051.

Hsu, K.L., Gao, X., Sorooshian, S., Gupta, H.V., 1997. Precipitation estimation from remotely sensed information using artificial neural networks. Journal of Applied Meteorology 36, 1176-1190.

Huffman, G.J., Bolvin, D.T., Nelkin, E.J., Wolff, D.B., Adler, R.F., Gu, G., Hong, Y., Bowman, K.P., Stocker, E.F., 2007. The TRMM multi satellite precipitation analysis (TMPA): Quasi-global, multiyear, combined-sensor precipitation estimates at fine scales. Journal of Hydrometeorology 8, 38-55.

Jiang, S.H., Ren, L.L., Yong, B., Yang, X.L., Shi, L., 2010. Evaluation of high-resolution satellite precipitation products with surface rain gauge observations from Laohahe basin in northern China. Water Science and Engineering 3, 405-417.

Jiang, S.H., Zhou, M., Ren, L.L., Cheng, X.R., Zhang, P.J., Evaluation of latest TMPA and CMORPH satellite precipitation products over Yellow River Basin. Water Science and Engineering 9, 87-96.

Jones, T. A., Stensrud, D.J., Wicker, L., Minnis, P., Palikonda, R., 2015. Simultaneous radar and satellite data storm-scale assimilation using an ensemble Kalman filter approach for 24 May 2011. *Mon. Wea. Rev.* 143, 165–194.

Joo, J., Kim, S., Park, M., Kim, J., 2015. Evaluation and calibration method proposal of RCP daily precipitation data. Journal of Korean Society of Hazard Mitigation 15, 79-91.

Joyce, R.J., Janowiak, J.E., Arkin, P.A., Xie, P., 2004. CMORPH: A method that produces global precipitation estimates from passive microwave and infrared data at high spatial and temporal resolution. Journal of Hydrometeorology 5, 487-503.

Katiraie-Boroujerdy, P.S., Nasrollahi, N., Hsu, K.L., Sorooshian, S., 2013. Evaluation of satellite-based precipitation estimation over Iran. Journal of arid environments 97, 205-219.

Kim, J., Han, H., Johnson, L. E., Lim, S., Cifelli, R., 2019. Hybrid machine learning framework for hydrological assessment. Journal of Hydrology 577, 123913.

Kim, J., Han, H., Kim, B., Chen, H., Lee, J., 2020. A high-resolution-satellite-based rainfall

erosivity map: a case study of the United States, Catena 193, 104602.

Kim, J., Joo, J., 2015. Characteristics of daily precipitation data based on the detailed climate change ensemble scenario depending on the regional climate models and the calibration. Journal of Korean Society of Hazard Mitigation 15, 261-272.

Kim, J., Park, M., Joo, J., 2015b. Comparison of characteristics and spatial distribution tendency of daily precipitation based on the regional climate models for the Korean Peninsula. Journal of Korean Society of Hazard Mitigation 15, 59-70.

Kim, J., Yoo, C., 2014. Use of a dual Kalman filter for real-time correction of mean field bias of radar rain rate. Journal of Hydrology 519, 2785-2796.

Kim, J., Yoo, C., Lim, S., Choi, J., 2015a Usefulness of relay-information-transfer for radar QPE. Journal of Hydrology 531, 308-319.

Li, M., Shao, Q.X., 2010. An improved statistical approach to merge satellite rainfall estimates and raingauge data. Journal of Hydrology 385, 51-64.

Liechti, T.C., Matos, J.P., Boillat. J.L., Schleiss, A.J., 2012. Comparison and evaluation of satellite derived precipitation products for hydrological modeling of the Zambezi River Basin. Hydrology and Earth System Sciences 16, 489-500.

Moazami, S., Golian, S., Hong, Y., Sheng, C., Kavianpour, M.R., 2016. Comprehensive evaluation of four high-resolution satellite precipitation products under diverse climate conditions in Iran. Hydrological Sciences Journal 61, 420-440.

Pan, M., Li, H., Wood, E., 2010. Assessing the skill of satellite-based precipitation estimates in hydrologic applications. Water Resources Research 46, W09535.

Peña Arancibia, J.L., van Dijk, A.I.J.M., Renzullo, L.J., Mulligan, M., 2013. Evaluation of precipitation estimation accuracy in reanalyses, satellite products, and an ensemble method

for regions in Australia and South and East Asia. J. Hydrometeorol. 14, 1323–1333.

Peng, F., Zhao, S., Chen, C., Cong, D., Wang, Y., Ouyang, H., 2020. Evaluation and comparison of the precipitation detection ability of multiple satellite products in a typical agriculture area of China. Atmospheric Research 236, 204814.

Romaguera, M., Hoekstra, A.Y., Su, Z., Krol, M.S., Salama, M., 2010. Potential of using remote sensing techniques for global assessment of water footprint of crops. Remote Sensing 2, 1177-1196.

Salio, P., Hobouchian, M.P., Skabar, Y.G., Vila, D., 2015. Evaluation of high-resolution satellite precipitation estimates over southern South America using a dense rain gauge network. Atmospheric Research 163, 146-161.

Sorooshian S., AghaKouchak A., Arkin P., Eylander J., Foufoula-Georgiou E., Harmon R., Hendrickx J. M., Imam B., Kuligowski R., Skahill B., Skofronick-Jackson G., 2011. Advancing the remote sensing of precipitation. Bulletin of the American Meteorological Society 92, 1271-1272.

Stampoulis, D., Anagnostou, E.N., 2012. Evaluation of global satellite rainfall products over continental Europe. Journal of Hydrometeorology 13, 588-603.

Sun, R., Yuan, H., Liu, X., Jiang, X., 2016. Evaluation of the latest satellite–gauge precipitation products and their hydrologic applications over the Huaihe River basin. Journal of Hydrology 536, 302-319.

Tan, M., Ibrahim, A., Duan, Z., Cracknell, A., Chaplot, V., 2015. Evaluation of six high-resolution satellite and ground-based precipitation products over Malaysia. Remote Sensing 7, 1504-1528.

Xie, P., Joyce, R., Wu, S., Yoo, S. H., Yarosh, Y., Sun, F., Lin, R., 2017. Reprocessed, bias-

corrected CMORPH global high-resolution precipitation estimates from 1998. J. Hydrometeorol. 18, 1617-1641.

Yao, J., Chen, Y., Yu, X., Zhao, Y., Guan, X., Yang, L., 2020. Evaluation of multiple gridded precipitation datasets for the arid region of northwestern China. Atmospheric Research 236, 104818.

List of tables

Table 1 Statistical and error metrics used for evaluation

Metrics	Acronym (Range)	Equation
Correlation coefficient	CC [-1, 1]	$\frac{\sum(P_e - \overline{P_e})(P_o - \overline{P_o})}{\sqrt{\sum(P_e - \overline{P_e})^2}\sqrt{\sum(P_o - \overline{P_o})^2}}$
Nash-Sutcliffe efficiency	NSE (-inf, 1]	$1 - \frac{\sum(P_e - P_o)^2}{\sum(P_o - \overline{P_o})^2}$
Percent-bias	PBIAS [-100, inf)	$\left(\sum(P_e - P_o)\right) \div \sum P_o \times 100\ (\%)$
Root mean square error	RMSE (-inf, inf)	$\sqrt{\frac{\sum(P_e - P_o)^2}{m}}$
Volume error	VE [-100, inf)	$\frac{\sum P_e - \sum P_o}{\sum P_o} \times 100\ (\%)$
Peak error	PE [-100, inf)	$\frac{P_{e,peak} - P_{o,peak}}{P_{o,peak}} \times 100\ (\%)$
Time error	TE [0, inf)	$\left(1 - \frac{n_{overlab}}{n_o}\right) \times 100\ (\%)$

Table 2 Precipitation contingency table

Detected	Observed	
	Yes	No
Yes	Hit (H)	False alarms (F)
No	Miss (M)	Null

List of figures

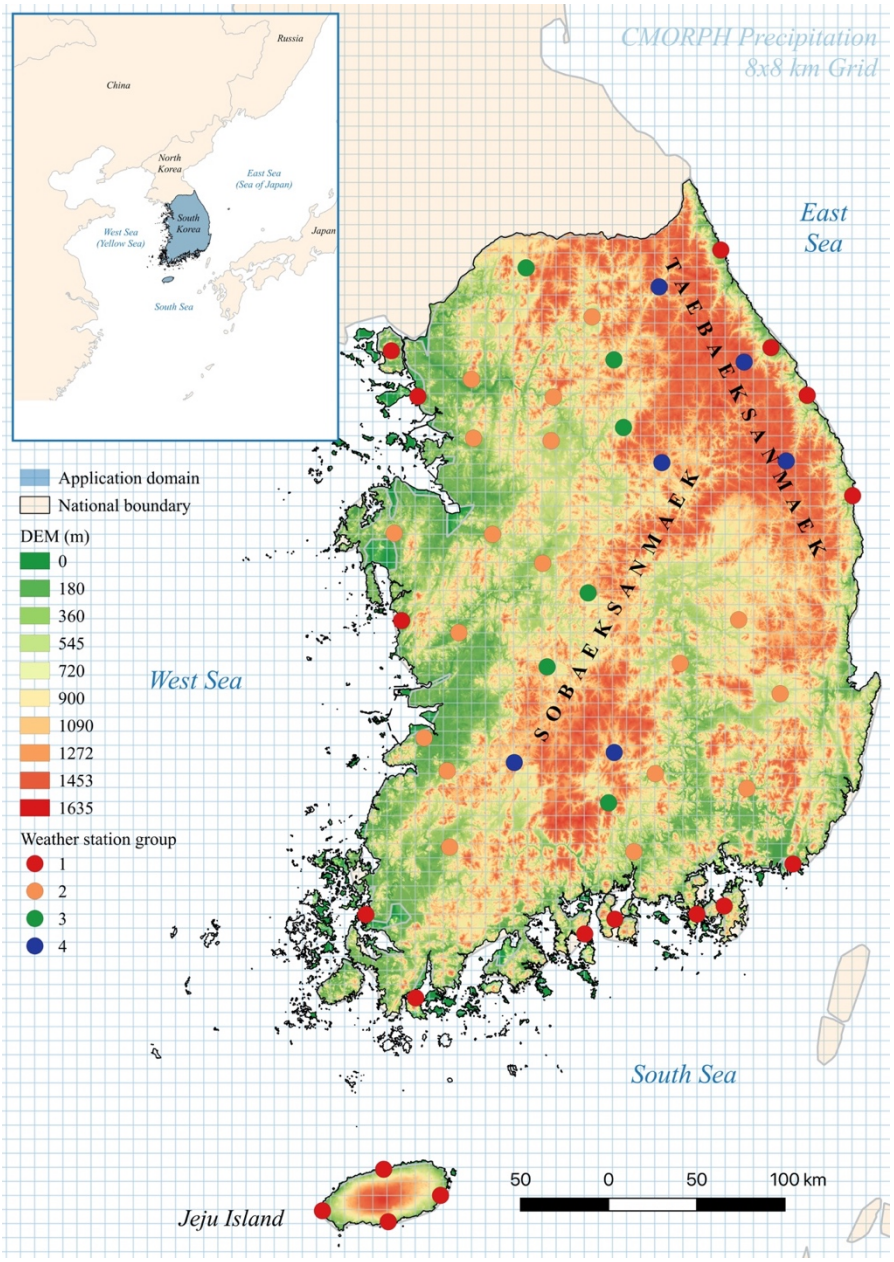

Fig. 1. The Korean Peninsula and the rain-gauge locations used in this study. The rain-gauges are grouped as Group1: Coastal area or island, Group2: elevation < 100m, Group3: elevation < 200m, and Group4: elevation > 200m.

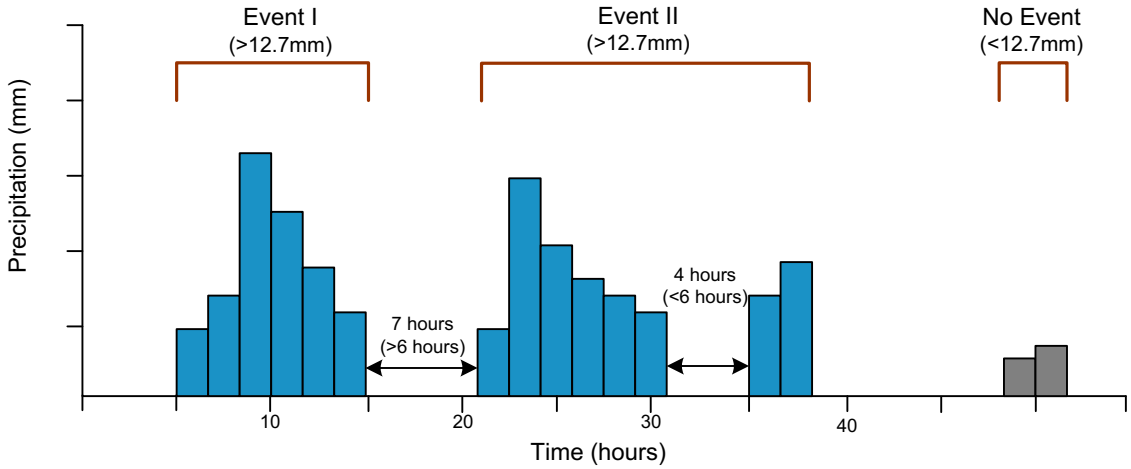

Fig. 2. A conceptual diagram of separating individual storm events.

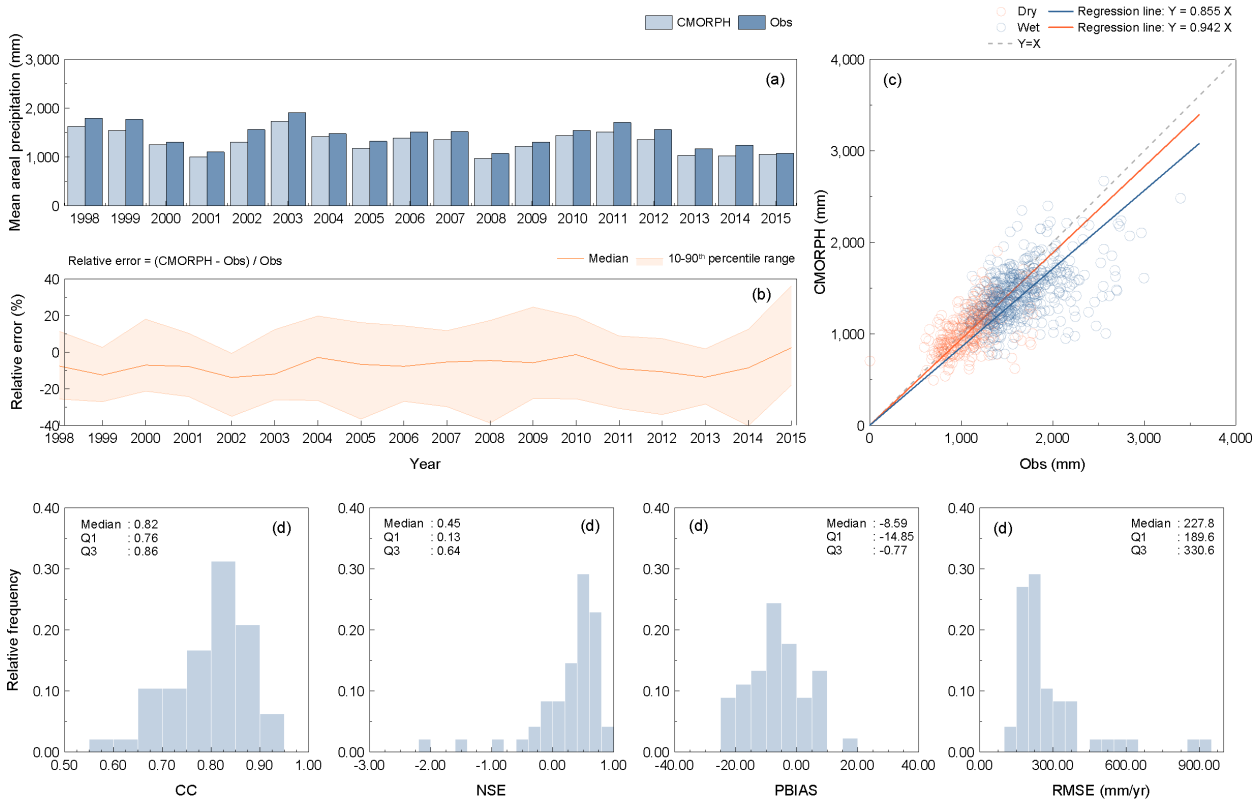

Fig. 3. Evaluation results of the annual precipitation: (a) a comparison of the mean annual precipitation of the rain-gauge and CMORPH, (b) relative error of each year for 18 years, (c) a scatter plot between the rain-gauge and CMORPH precipitation for wet and dry years, a circle indicates the annual precipitation at a rain-gauge location in a year, and orange and blue denote a dry and wet year respectively, and (d) PDFs of the statistical metrics (CC, NSE, PBAIS, and RMSE).

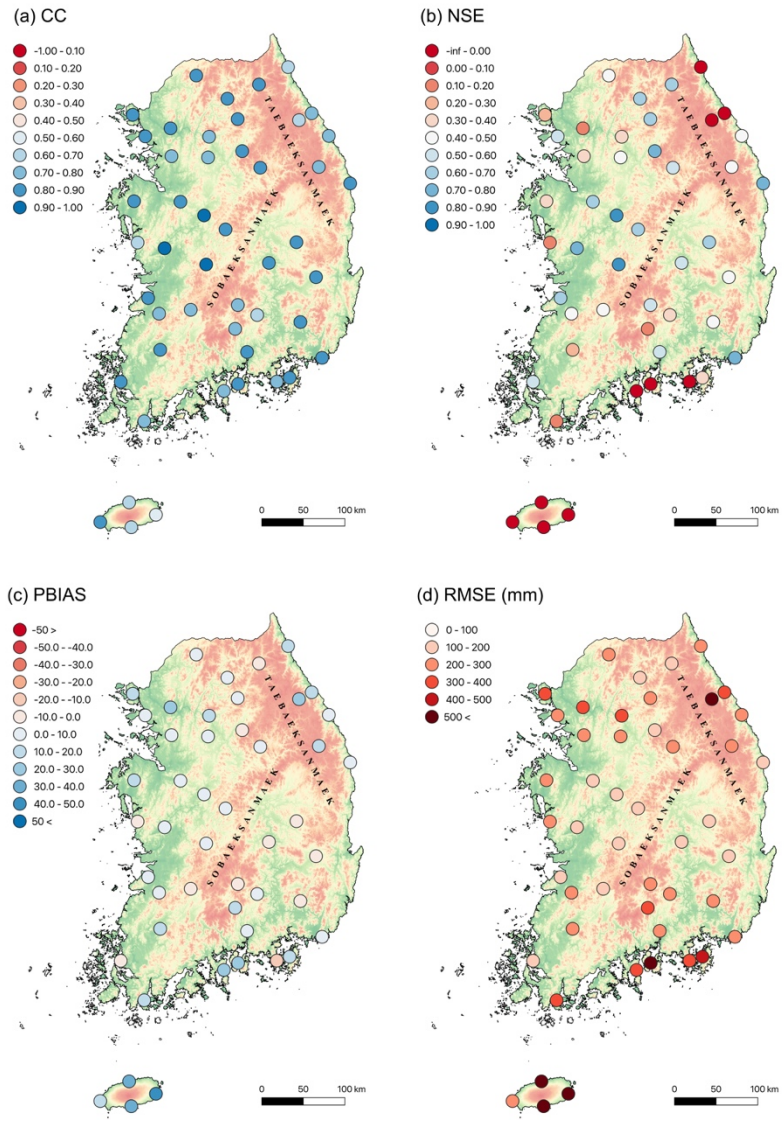

Fig. 4. Spatial distributions of the statistical metrics of the annual precipitation: (a) CC, (b) NSE, (c) PBIAS, and (d) RMSE.

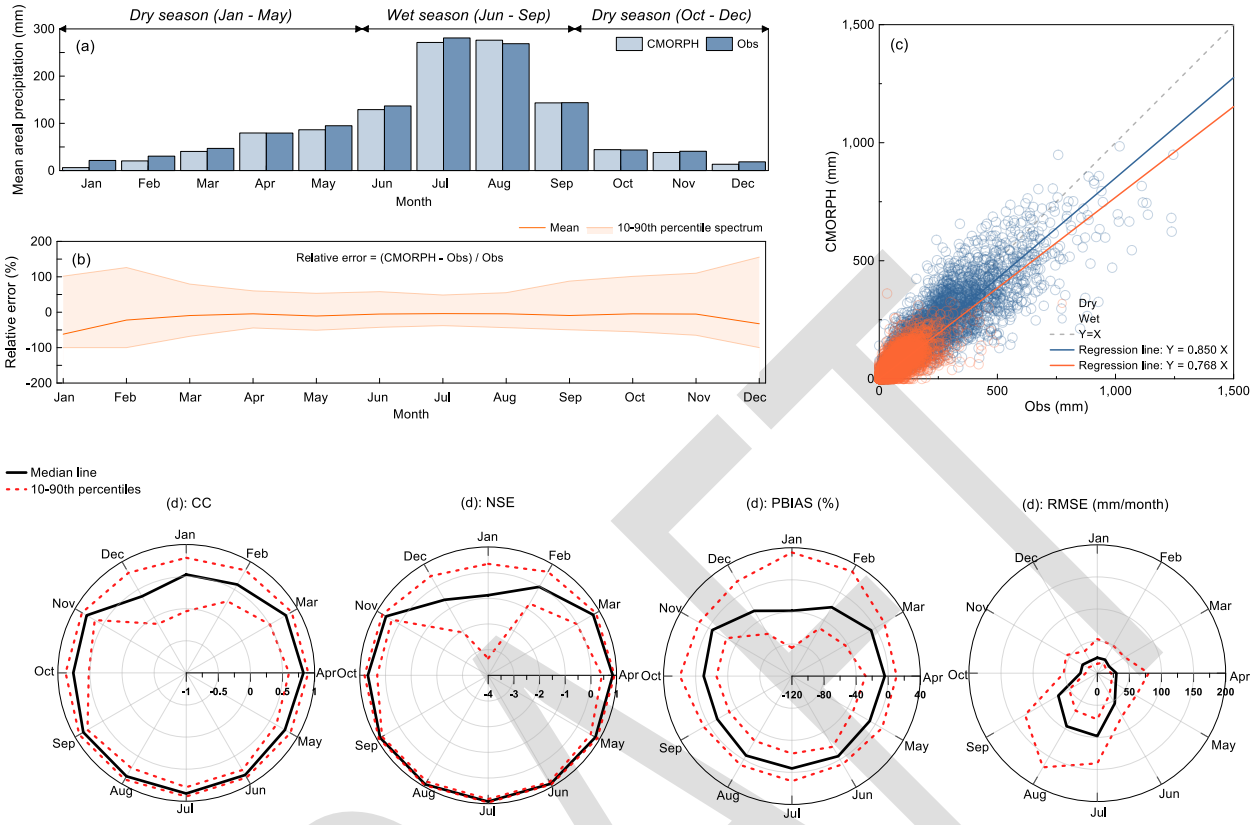

Fig. 5. Evaluation results of the monthly precipitation: (a) a comparison of mean monthly precipitation of the rain-gauge and CMORPH, (b) relative error (c) a scatter plot between the rain-gauge and CMORPH monthly precipitation for wet and dry years, and (d) radial graphs of the statistical metrics (CC, NSE, PBAIS, and RMSE).

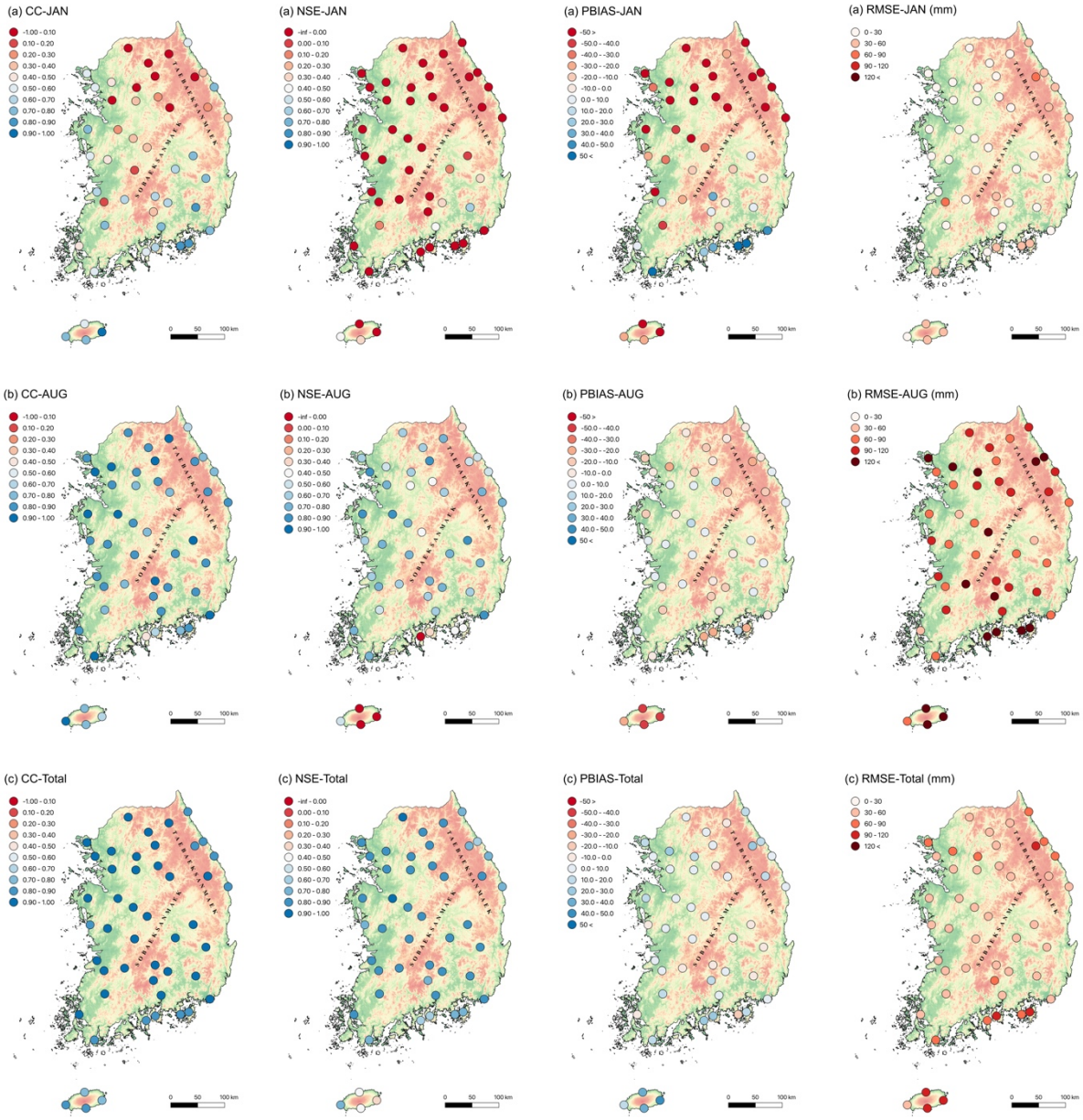

Fig. 6. Spatial distributions of the statistical metrics of the monthly precipitation: (a) January: a dry/winter month, (b) August: a wet month, and (c) Total.

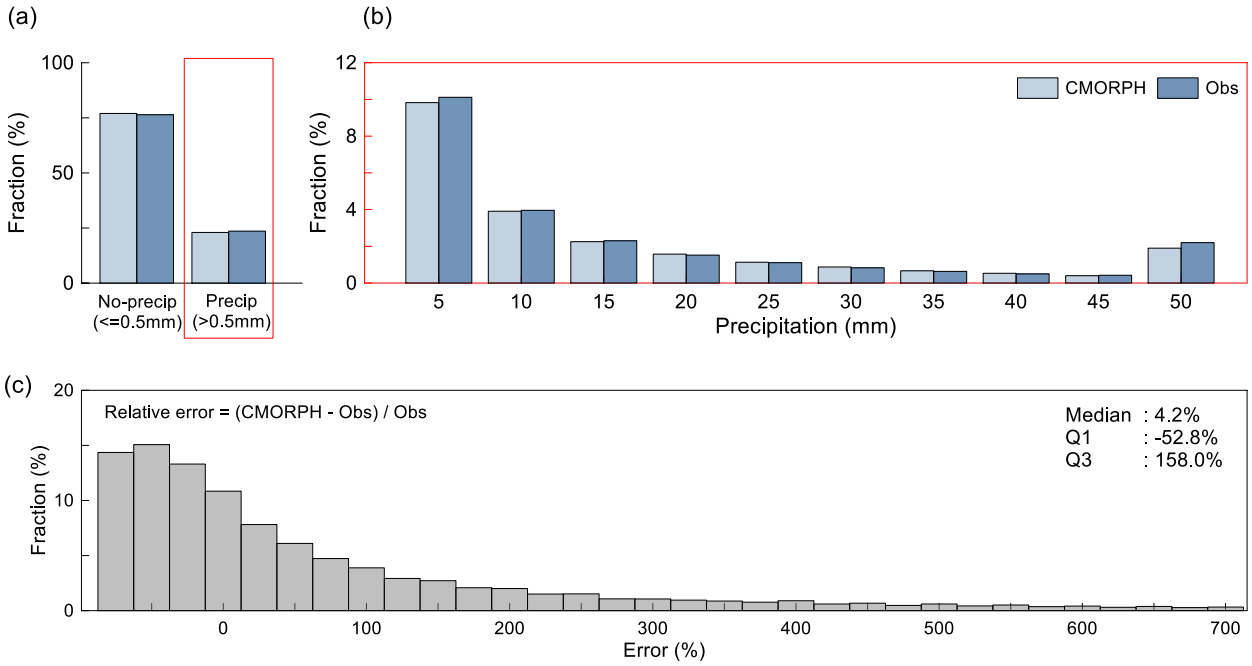

Fig. 7. Evaluation results of the daily precipitation: (a) the fractions of precipitation and no-precipitation from the rain-gauge and CMORPH, (b) the distribution of the fractions by precipitation interval, and (c) the distribution of relative errors.

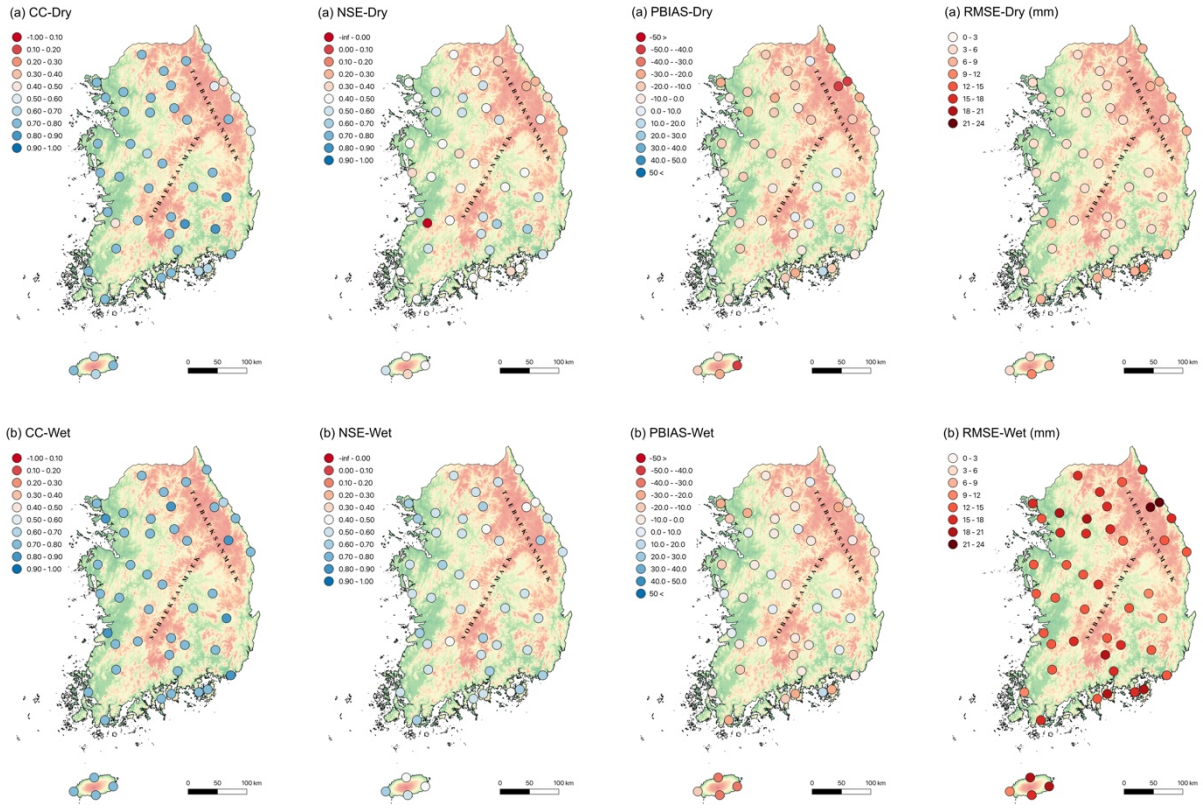

Fig. 8. Spatial distributions of the statistical metrics of the daily precipitation: (a) for a dry season and (b) for a wet season.

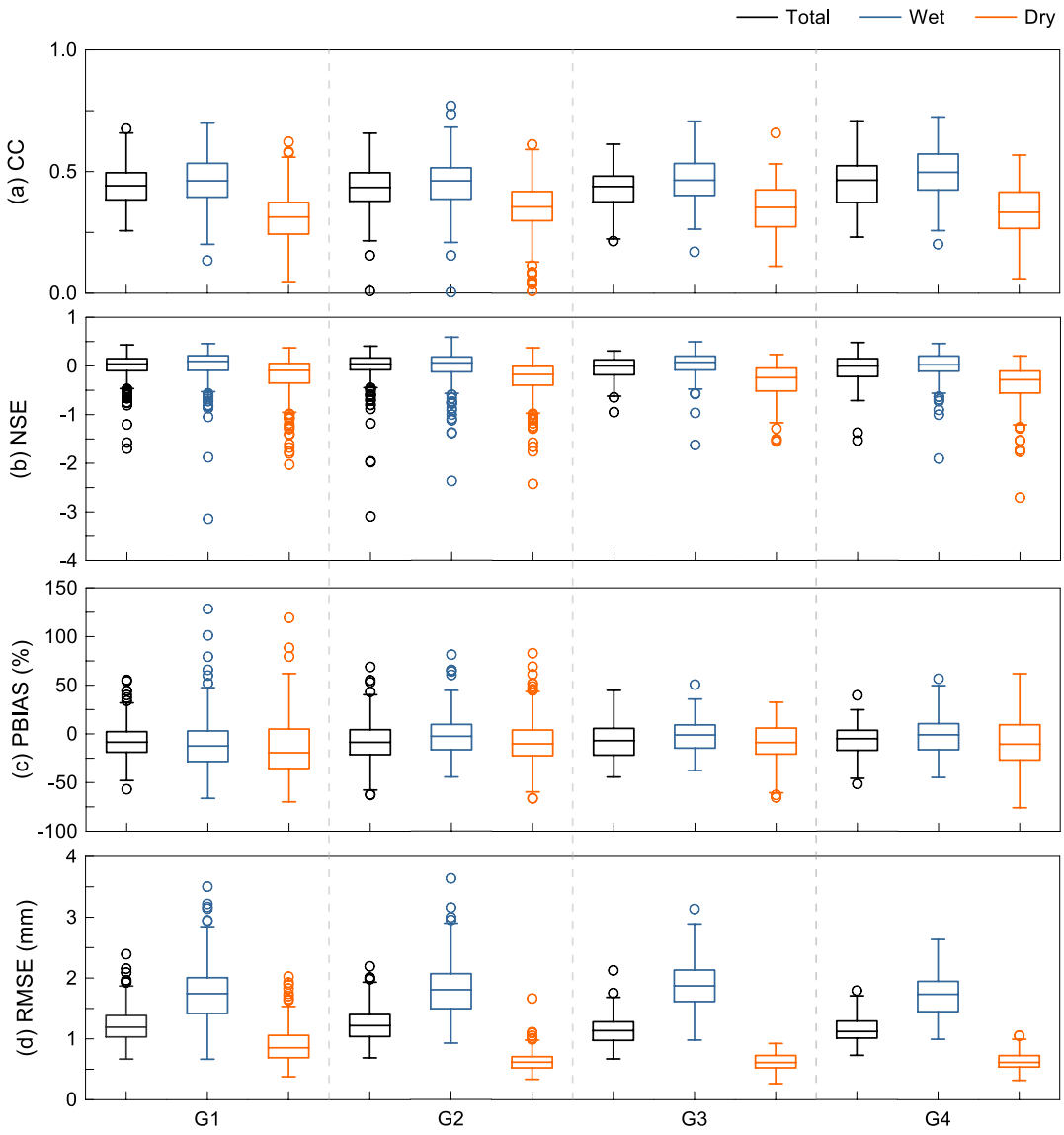

Fig. 9. The Box and Whisker plot of the statistics metrics of the hourly precipitation for the four groups and seasons: (a) CC, (b) NSE, (c) PBAIS, and (d) RMSE. Each box ranges from the lower quartile (25th) to the upper quartile (75th). The middle line indicates the median value in the box. The whiskers extend out to the largest and smallest values within 1.5 times the interquartile range. The circle presents the points beyond the whiskers.

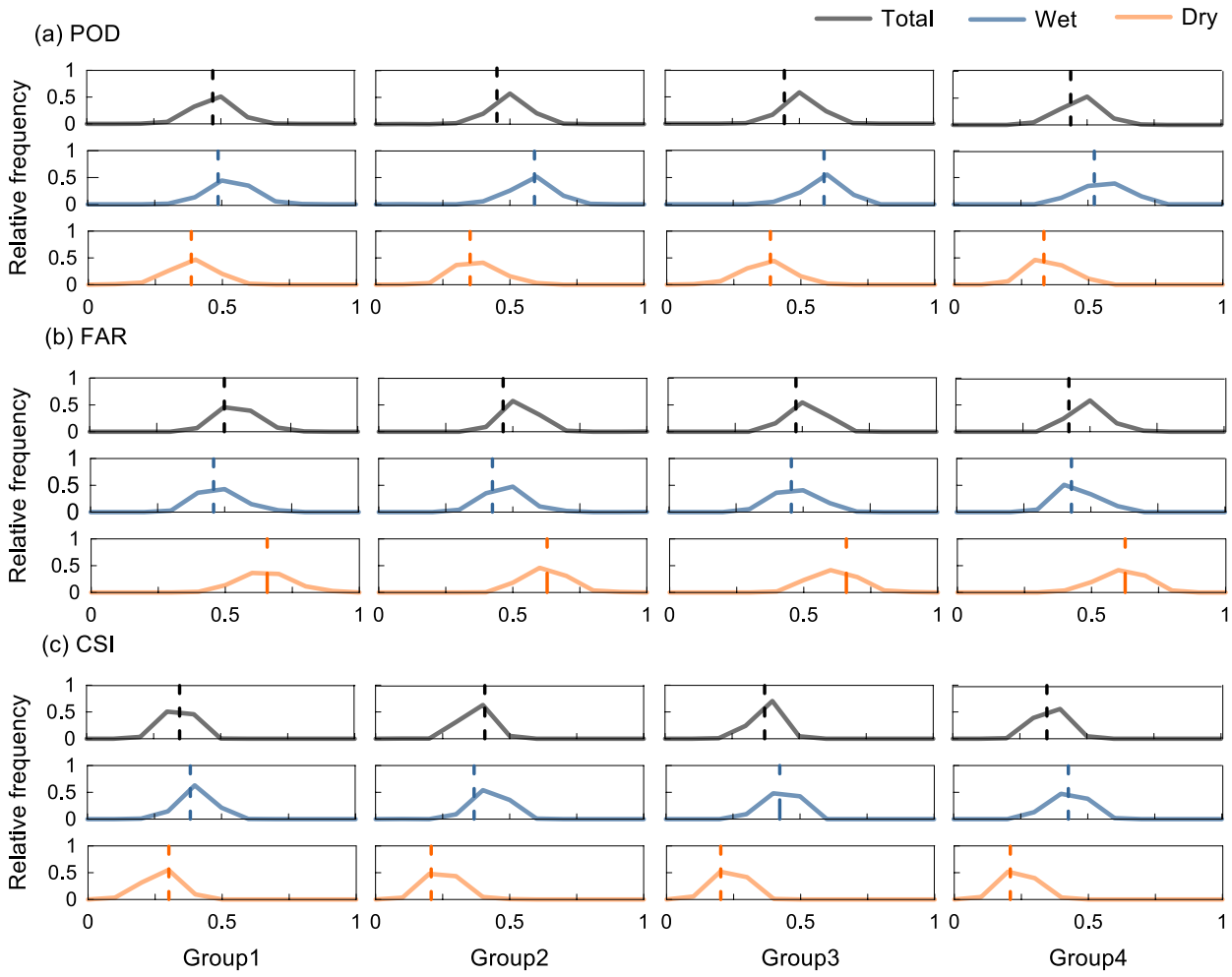

Fig. 10. PDFs of the categorical metrics for the four groups and seasons: (a) POD, (b) FAR, and (c) CSI. Each box shows the relative frequency of each metric, and the dotted vertical line indicates the mean value of the index. These results do not consider precipitation intensity.

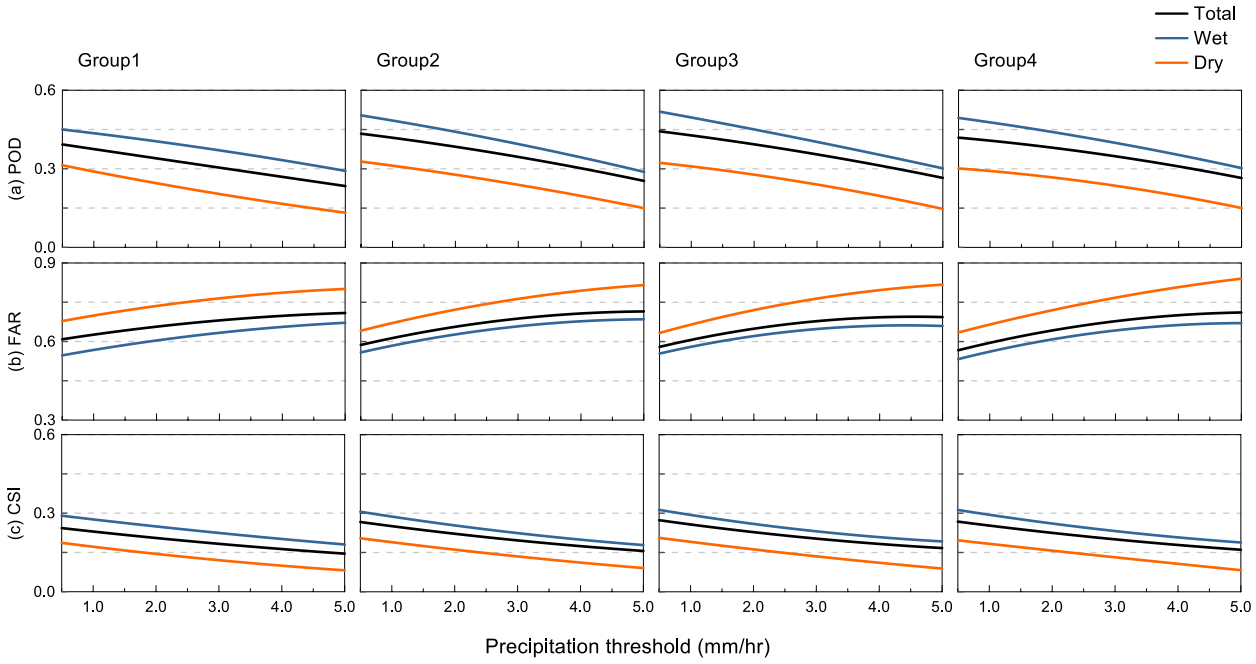

Fig. 11. Categorical metrics results considering the precipitation intensity for the four groups and seasons: (a) POD, (b) FAR, and (C) CSI.

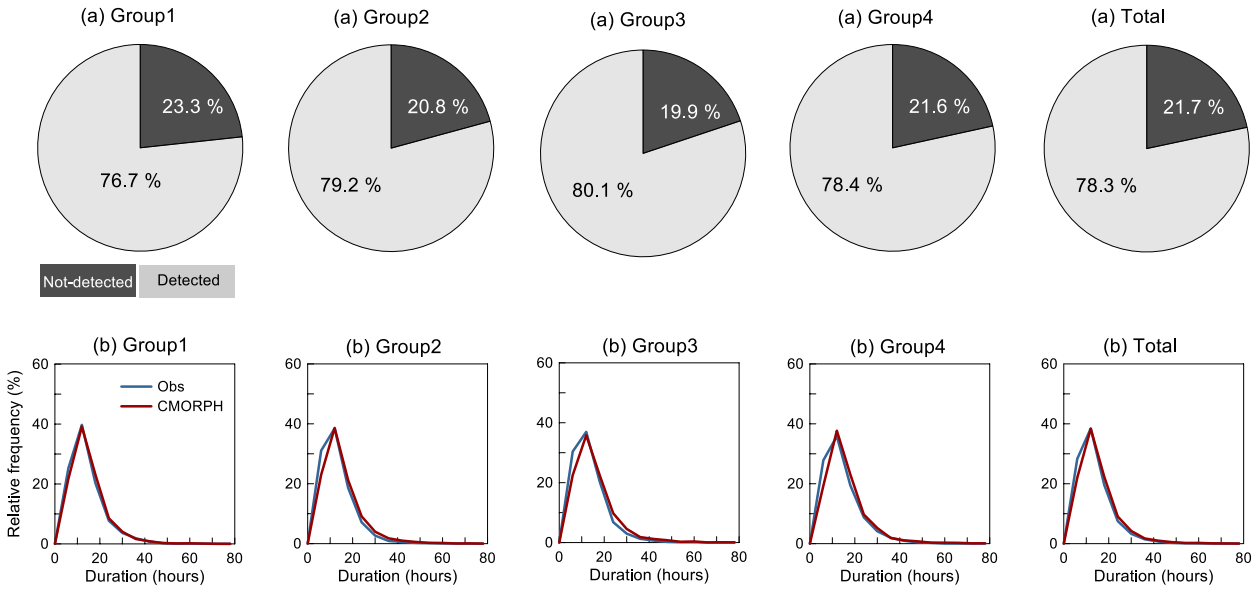

Fig. 12. Evaluation results of the event-based precipitation: (a) the fractions of not-detected and detected cases and (b) the PDFs of durations of a storm event.

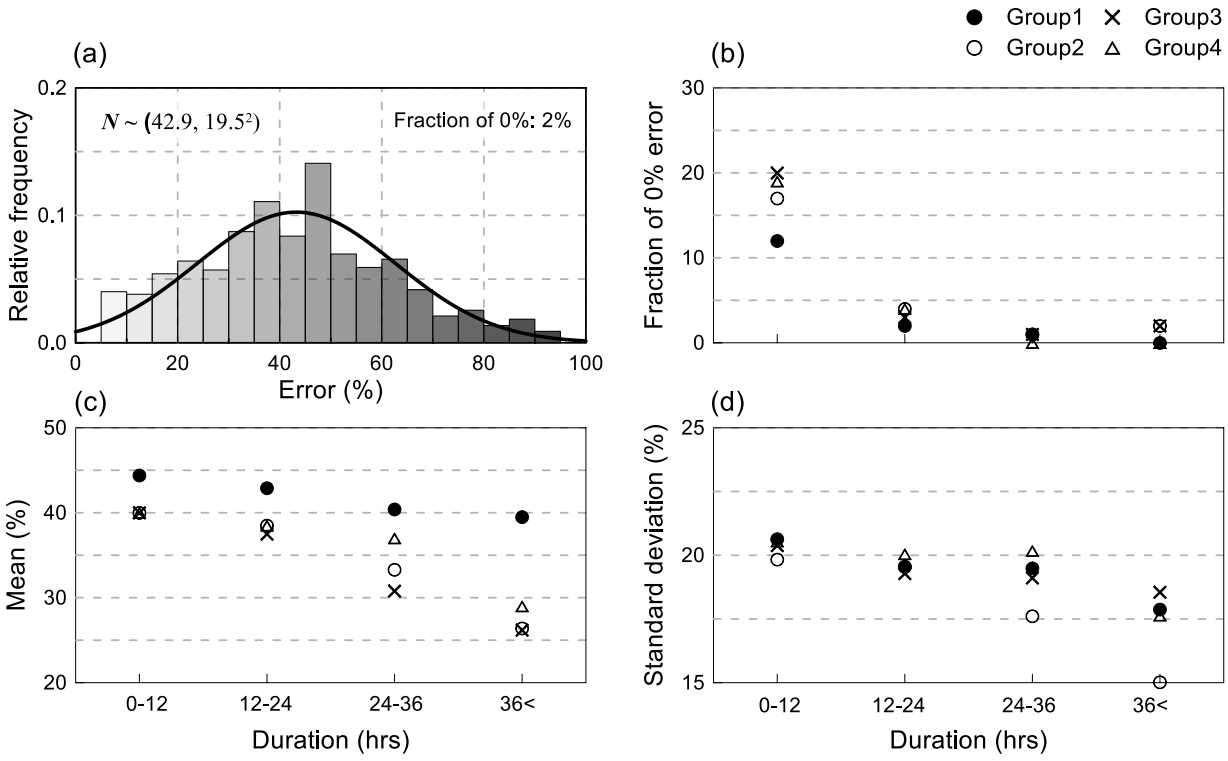

Fig. 13. Timing error results: (a) the PDF of the timing error for 12<d<24 in Group1, (b) a fraction of 0% timing error cases by the duration, (c) the mean values of the PDFs by duration, and (d) the standard deviations of the PDFs by duration.

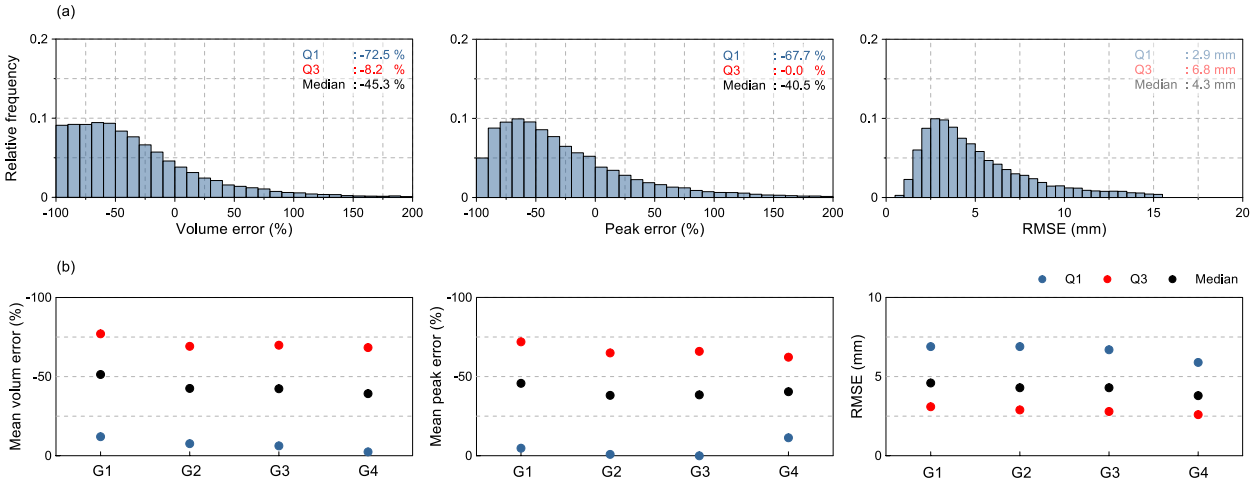

Fig. 14. Evaluation results of total volume error, peak error, and RMSE from detected storm events by group: (a) the PDFs of each error and (b) the 1st and 3rd quantiles and median values of the PDFs.